Tail-induced attraction between nucleosome core particles

F. Mühlbacher,[1] H. Schiessel,[2] and C. Holm[1,3]
[1]*Max-Planck-Institut für Polymerforschung, Theory Group, PO Box 3147, D-55021, Mainz, Germany*
[2]*Instituut-Lorentz, Universiteit Leiden, Postbus 9506, 2300 RA Leiden, The Netherlands*
[3]*FIAS, JW Goethe-University, Max-von-Laue Strasse 1, D-68438 Frankfurt/M, Germany*
(Received 6 June 2006; published 27 September 2006)

We study a possible electrostatic mechanism underlying the compaction of DNA inside the nuclei of eucaryotes: the tail-bridging effect between nucleosomes, the fundamental DNA packaging units of the chromatin complex. As a simple model of the nucleosome we introduce the eight-tail colloid, a charged sphere with eight oppositely charged, flexible, grafted chains that represent the terminal histone tails. We show that our complexes attract each other via the formation of chain bridges and contrast this to the effect of attraction via charge patches. We demonstrate that the attraction between eight-tail colloids can be tuned by changing the fraction of charged monomers on the tails. This suggests a physical mechanism of chromatin compaction where the degree of DNA condensation is controlled via biochemical means, namely the acetylation and deacetylation of lysines in the histone tails.

DOI: 10.1103/PhysRevE.74.031919 PACS number(s): 87.15.La, 82.37.Rs, 05.40.−a

I. INTRODUCTION

Plant and animal (eucaryotic) DNA is meters long but has to fit inside micron-sized nuclei. At the same time a considerable fraction of the genetic code stored within the highly compacted DNA has to be accessible to the cellular machinery. To achieve this remarkable task, the compacted DNA is folded in a hierarchical fashion [1]. At the first step two turns of DNA are wrapped around cylinders made from eight histone proteins. This results in a string of cylindrical DNA spools about 10 nm in diameter and 6 nm in height, each repeating unit being called a nucleosome [2]. As the next compaction level one posits typically the chromatin fiber with a diameter of about 30 nm which again forms higher order structures such as loops. The density of such structures varies along the fiber and in the course of the cell cycle and is presumably directly related to the genetic activity with the dense regions corresponding to "silenced" parts [3].

How does a eucaryotic cell cope with the challenge of combining high compaction and (selective) accessibility at the same time? Recent experiments and theories give us an idea of how the nucleosome is meticulously designed to face that challenge. In principle, when DNA is wrapped onto the protein cylinder, it is in a "closed" state inaccessible for DNA binding proteins. However, thermal fluctuations open a window of opportunity for such proteins via the unwrapping of either one of the two turns [4–7] or via a corkscrew sliding of the octamer *along* the DNA chain [8–10]. Active sliding of nucleosomes along DNA is induced via remodeling complexes [11].

At the next compaction levels the situation is less clear. The chromatin fiber has roughly 40 times shorter contour length than that of the DNA chain that it contains but it is, at the same time, much stiffer than the naked DNA. The resulting coil size of the chromatin fiber would still be much larger than the diameter of the cell nucleus (cf. footnote 8 in Ref. [12]). This makes nucleosome-nucleosome attraction necessary as a further means of compaction, a mechanism that should be tunable allowing dense and transcriptionally passive fiber sections as well as more open and active ones.

Important questions ensue: Do nucleosomes attract each other, and what is then the underlying mechanism? And how can this interaction be tuned for individual nucleosomes? Recent experiments indeed point towards a simple physical mechanism that causes attraction between nucleosomes: the histone tail bridging [13–15]. The histone tails are flexible extensions of the eight core proteins that carry several positively charged residues [2,16] and extend considerably outside the globular part of the nucleosome. Mangenot *et al.* [13] studied dilute solutions of nucleosome core particles (NCPs; the particles that are left when the nonadsorbed "linker" DNA is digested away). From small angle x-ray scattering it was shown that NCPs change their size with increasing salt concentration: At around 50 mM monovalent salt the radius of gyration increases slightly (from 43 to 45 Å) and, at the same time, the maximal extension of the particle increases significantly (from 140 to 160 Å). This observation was attributed to the desorption of the cationic histone tails from the NCP that carries an overall negative charge (cf. Ref. [1]). Osmometric measurements [14] detected around the salt concentration where the tails desorb an attractive contribution to the interaction between the NCPs, manifest in a considerable drop of the second virial coefficient. The coincidence of the ionic strengths where both effects occur led Mangenot *et al.* to suggest that it is the tails that are mainly involved in the attractive interaction. This picture was supported by another study [15] where it was shown that there there is no attraction for tailless NCPs.

Theories for nucleosomal attraction come to diverging conclusions. Attraction between simplified model nucleosomes has been reported in a nucleosome model [17,18,20] that ignored the tails. The nucleosome was modeled by a positively charged sphere (representing the protein core) and a semiflexible anionic chain (the DNA) wrapped around. The interaction between two such complexes (at zero temperature) showed an attraction at intermediate salt concentrations that leads to a nonmonotonic behavior of the second virial coefficient with the minimum reflecting the attractive regime (cf. Fig. 4 in Ref. [17]). In a more general context, this kind

of nonmonotonic interaction can be interpreted to belong to the class of attraction induced by correlations between charge patches [19]. An example provides a computer simulation of Allahyarov *et al.* [20] who studied the interaction between spherical model proteins decorated with charge patches; the second virial coefficient featured a nonmonotonic behavior as a function of ionic strength.

On the other hand, Podgornik [21] focused on tail bridging in a model where the NCP was represented by a pointlike particle with an oppositely charged flexible chain. This system showed NCP-NCP attraction but no nonmonotonic behavior of the second virial coefficient. Thus the question arises whether it is really the tail bridging that causes the attraction between NCPs observed at intermediate salt concentrations. Earlier studies had already established that polyelectrolyte chains form bridges between charged planar surfaces [22,23] and colloids [24,25] (carrying charges of a sign opposite to the chain) that cause attraction. An interesting demonstration of the difference between attraction due to charge correlations and due to bridging was given by continuously changing the stiffness of the entropic springs connecting neighboring monomers of the polyelectrolyte chain [22]: A vanishing spring constant leads to the usual repulsive double layer force due to the counterions in between the walls, harder springs lead to polyelectrolyte chains that cause bridging, and finally very hard springs induce a collapse of each chain onto a point which corresponds to multivalent counterions that cause attraction due to charge correlations. Both effects, bridging and charge correlations, lead to attractive regimes that were clearly separated from each other (cf., e.g., Fig. 8 in Ref. [22]). Of interest is also the observation that bridging interactions induced by free chains are very similar to those of chains that are grafted on either surface [23].

Although those earlier studies provided already substantial insight into bridging interactions, several issues remained open, especially in the light of the new experimental [13,14] and theoretical studies [16,18]. The purpose of the current study (which presents an extended, more detailed version of Ref. [12]) is fourfold: (i) to introduce a minimal model for NCPs that includes its tails, (ii) to test whether such a model shows attraction with a nonmonotonically varying second virial coefficient, (iii) to put tail bridging on a stronger footing and demonstrate how the ensuing effect is qualitatively different from attraction through charge patches, and (iv) to demonstrate how tail bridging can be used to facilitate control of nucleosomal interaction which in turn might affect the compaction state of chromatin.

In the next section we introduce our NCP model, the eight-tail colloid. In Sec. III we present single colloid properties. The following sections focus on the interaction between two colloids: the pair potential and second virial coefficient for eight-tail colloids and simplified colloid models in Sec. IV, details of the tail bridging in Sec. V, and the dependence of the interaction on the tail charge fraction in Sec. VI. Section VII presents a variant of the eight-tail colloid where the tails are attached via freely floating anchors. Finally, the last section presents discussions and conclusions, especially regarding the role of tail bridging within the chromatin complex.

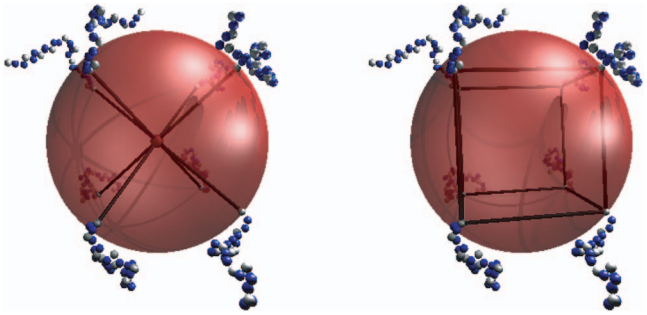

FIG. 1. (Color online) The eight-tail colloid. Eight polyelectrolyte chains are grafted onto the surface of an oppositely charged sphere. Both pictures show the identical colloid but highlight a different set of stiff harmonic bonds. The first set on the left is given by eight bonds from the colloidal center to the grafted monomers that enforce them to lie on the surface of the colloidal sphere. The second set of bonds is shown on the right that act between neighboring grafted monomers so that they sit on the vertices of a cube.

II. EIGHT-TAIL MODEL FOR THE NCP

We give in the following a more detailed presentation of our NCP model, the eight-tail colloid, that we introduced in Ref. [12]. It consists of a sphere with eight end-grafted polymer chains, cf. Fig. 1. The sphere represents here the NCP without the tails, i.e., the globular histone octamer with the DNA wrapped around. The sphere carries a negative charge $-Z$ homogeneously smeared out over the surface to account for the net charge of the DNA-octamer complex; the negative sign reflects the fact that the DNA overcharges the cationic protein core [1]. The sphere radius is chosen to be $a=15\sigma$ with $\sigma=3.5$ Å being our unit length.

The eight histone tails are modeled by flexible chains end-grafted onto the sphere. Each chain consists of 28 monomers of size σ where each third monomer carries a positive unit charge, the rest being neutral. All these parameters have been chosen to match closely the values of the NCP; our tails feature the average length of the *N*-terminal tails whose lengths range from 15 residues (histone H2A) to 44 (H3).

The bonding interactions of the neighboring monomers of the chains were modeled using the finitely extensible nonlinear elastic (FENE) potential [26]. Excluded volume of the tail monomers and the cores are described by purely repulsive Lennard-Jones (LJ) potentials. The corresponding interaction between two tail monomers is given by

$$V_{lj}^{mm}(r) = 4\epsilon_{LJ}\left[\left(\frac{\sigma}{r}\right)^{12} - \left(\frac{\sigma}{r}\right)^{6} + \frac{1}{4}\right] \tag{1}$$

for distances $r \leqslant r_{cut}^{mm}$ with $r_{cut}^{mm}=2^{1/6}\sigma$ and zero otherwise. The interaction between a tail monomer and a core of radius a is given by the slightly modified expression

$$V_{lj}^{cm}(r) = 4\epsilon_{LJ}\left[\left(\frac{\sigma}{r-a}\right)^{12} - \left(\frac{\sigma}{r-a}\right)^{6} + \frac{1}{4}\right] \tag{2}$$

for distances $a<r\leqslant r_{cut}^{cm}$ with $r_{cut}^{cm}=2^{1/6}\sigma+a$. Again the potential is 0 for $r>r_{cut}^{cm}$. Since the positions of the cores are fixed in our simulations and are always larger than the core diam-

eter, excluded volume interactions between the cores have not to be specified here.

We fix the grafted chains onto the sphere surface at the vertices of a cube. The grafting potential

$$V_{\text{graft}}(r) = 1/2k_{\text{graft}}(r-a)^2 \tag{3}$$

is applied between one end monomer of each chain and the center of the sphere, as illustrated on the left side of Fig. 1. Here r represents the distance between the grafted monomer and the core, k_{graft} denotes the spring constant. Similarly we apply a potential to keep constant relative distances r between grafted monomers of neighboring tails:

$$V_{\text{cube}}(r) = 1/2k_{\text{cube}}(r-r_{\text{cube}})^2, \tag{4}$$

with r_{cube} being the length of an edge of the resulting cube, as indicated on the right of Fig. 1.

In addition, all charged monomers and the central sphere experience an electrostatic interaction via the standard Debye-Hückel (DH) theory with an inverse screening length $\kappa=\sqrt{4\pi l_B c_s}$, where c_s denotes the monovalent salt concentration and $l_B=2\sigma$ sets the Bjerrum length in water at room temperature ($l_B=e^2/\epsilon k_B T$; e: electron charge; ϵ: dielectric constant of solvent; $k_B T$: thermal energy) [27]. Since we use a DH potential, we need to use an effective value $-Z_{\text{eff}}$ for the central charge to account for charge renormalization [28]. Inside a cell nucleus the salt concentration is about 100 mM of sodium chloride, which corresponds to a value of κ of approximately $0.4\sigma^{-1}$. The effective pair potential for two monomers, which can be treated as pointlike charges, is then given by

$$\frac{V_{DH}^{mm}(r)}{k_B T} = l_B \frac{\exp(-\kappa r)}{r}. \tag{5}$$

In the case of the interaction of a monomer and a core the interaction becomes

$$\frac{V_{DH}^{mc}(r)}{k_B T} = Z l_B \frac{\exp(\kappa a)}{1+\kappa a}\frac{\exp(-\kappa r)}{r}. \tag{6}$$

Finally the core-core interaction can be written as

$$\frac{V_{DH}^{cc}(r)}{k_B T} = Z l_B \frac{\exp(2\kappa a)}{(1+\kappa a)^2}\frac{\exp(-\kappa r)}{r}. \tag{7}$$

In the simulations presented in this work, l_B was chosen to be 2σ. This value corresponds to the Bjerrum length of water, which is about 7 Å.

A velocity Verlet algorithm with a standard Langevin thermostat [29] is used to integrate the equation of motion (time step 0.01τ, friction coefficient $\Gamma=\tau^{-1}$, Lennard-Jones time unit τ):

$$m\ddot{r} = -\nabla V(r) - \Gamma\dot{r} + \xi(t). \tag{8}$$

Here r and m denote the position and the mass of a particle. $V(r)$ describes the corresponding potential and $\xi(t)$ the random collisions of the surrounding medium. $\xi(t)$ is a δ-correlated Gaussian noise term with $\langle\xi\rangle=0$ and

TABLE I. Simulation parameters.

Parameter	Symbol	value
Unit length	σ	3.5 Å
Bjerrum length	l_B	2σ
Time step	Δt	0.01τ
Thermal energy	kT	ϵ_{LJ}
Core central charge	Z	150
Monomer charge		$-e_0$
Core radius	a	15σ
Friction constant	Γ	$\epsilon_{LJ}\cdot\tau/\sigma^2$
Parameters for the		
Graft potential	k_{graft}	$2\epsilon_{LJ}/\sigma^2$
	r_{graft}	a
Cube potential	k_{cube}	$2\epsilon_{LJ}/\sigma^2$
	r_{cube}	17.3σ
FENE potential	k_{FENE}	$7\epsilon_{LJ}/\sigma^2$
	r_{FENE}	2σ
Monomers per chain	N	28
Charged monomers per chain		10

$$\langle\xi_i(t)\xi_j(t')\rangle = 6kT\Gamma\delta_{ij}\delta(t-t'). \tag{9}$$

ξ is adjusted via the fluctuation-dissipation theorem, for the simulations presented here Γ was set to 1 $\frac{\epsilon_{LJ}\cdot\tau}{\sigma^2}$.

A summary of the simulation parameters is provided in Table I. These values were used throughout the simulations unless stated differently.

III. PROPERTIES OF SINGLE EIGHT-TAIL COLLOIDS

Figure 2 depicts the diameter of a single eight-tail colloid as a function of κa and Z, with $-Z$ being the charge on the sphere. The diameter is defined as the thermally averaged maximal distance D_{max} between the two most distant tail monomers:

$$D_{max} = \langle\sqrt{(\vec{r}_i-\vec{r}_j)^2}\rangle \tag{10}$$

Here i and j denote the two monomers of the complex that—at the given time—have the maximal distance from each other. We varied Z from 0 to 300 and κ from 0 to 1, corresponding to salt concentrations from 0 to 5 mol. We obtained D_{max} at each pair of parameters by performing a simulation run for 10^6 time steps, discarding the first 2.5×10^5 time steps to allow the system to equilibrate.

For $Z=0$ and small values of κ, i.e., at low ionic strength, the eight tails are extended, radially pointing away from the center of the complex, cf. the example at $\kappa a=0$. For large values of Z, say, for $Z>100$, and small κ the tails are condensed onto the sphere, cf. the configuration at $Z=300$ and $\kappa a=0$. Increasing the screening leads finally in both cases to structures where the chains form random self-avoiding polymer coils as the ones in the example configuration at the left of Fig. 2.

Consider a complex with condensed chains for some low κ value and some $Z>100$. With increasing κ the chains de-

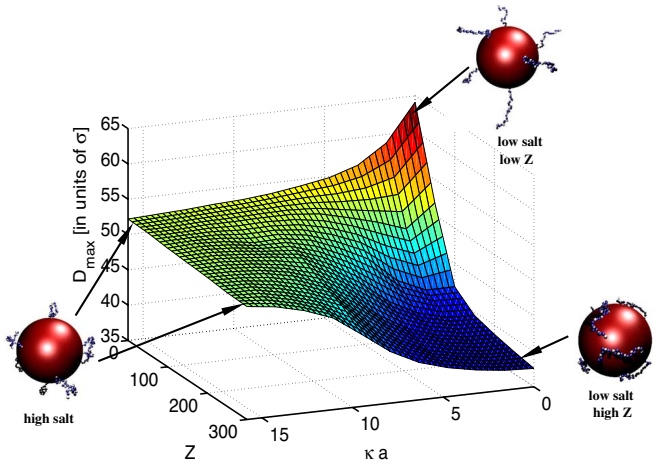

FIG. 2. (Color online) Average diameter D_{max} of the eight-tail complex—defined in Eq. (10)—as a function of κa and Z. For a neutral sphere, $Z=0$, the colloid is extended in the absence of salt, $\kappa a=0$ (cf. the example configuration on the upper right corner) and decreases with increasing salt to a structure like the one depicted on the left. A highly charged complex, e.g., $Z=300$, features collapsed tails for no salt (cf. the colloid on the lower right) and shows for high salt, i.e., strong screening, also configurations like the one shown on the left.

sorb around a certain κ value which is larger for larger Z. A comparison of our curves for $Z>100$ with the experimental ones [13] shows a qualitatively similar chain unfolding scenario. Furthermore, by choosing $Z=150$ we are able to match closely the experimental and the simulation values of c_s at which tail unfolding takes place. In the following we will therefore always use this value as our Z_{eff}.

Figure 3 presents the densities of the tail monomers above the surface of the sphere with $Z=150$ for different salt concentrations. In the absence of salt, $\kappa\sigma=0$, most monomers are located very close to the surface such that the density is practically zero for distance beyond 5σ. Around physiological conditions, $\kappa\sigma=0.4$ there is a small but finite probability to find monomers also further apart from the surface up to a distance of, say, 10σ. Finally, at stronger screening the tails are essentially desorbed which is reflected by a broad distribution of the monomer density.

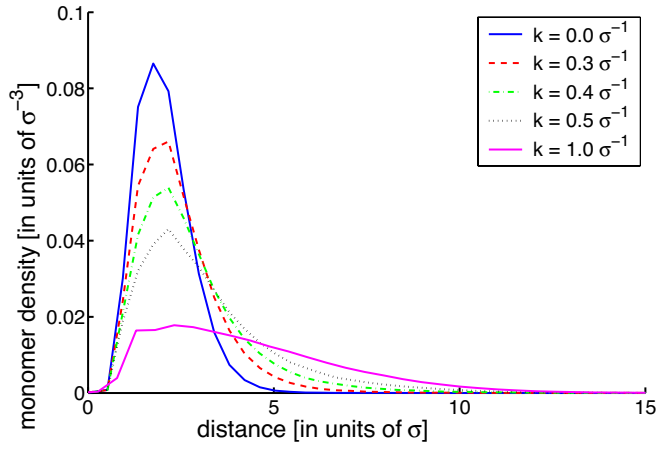

FIG. 3. (Color online) The radial monomer densities of the tails grafted on a sphere with $Z=150$ as a function of distance above its surface. The different curves correspond to different salt concentrations leading to $\kappa\sigma=0$ (solid line), $\kappa\sigma=0.3$ (dashed line), $\kappa\sigma=0.4$ (dashed-dotted line), $\kappa\sigma=0.5$ (dotted line), and $\kappa\sigma=1.0$ (solid line).

IV. INTERACTION OF COMPLEXES

We next determine the pair potential between eight-tail complexes and study how this potential is affected by a change in the ionic conditions. In order to do so, we fix two complexes at a constant distance from each other and run ten MD simulations of 10^6 time steps with different starting conditions. 2.5×10^5 time steps are removed for equilibration, for the rest of the time the interacting force on the cores is measured every 250 time steps. This results in 3000 data points for each of the ten samples. Note that the complexes are allowed to rotate freely around their center of mass. The mean interaction force between the two complexes is then determined as the force projected on the connecting line of the two centers:

$$F_{\text{int}} = \frac{1}{2}\langle(\vec{F}_2 - \vec{F}_1)\cdot\vec{e}_{12}\rangle. \tag{11}$$

$\vec{F}_i$ is the effective force felt by the core of complex i and $\vec{e}_{12}$ denotes the unit vector from the center of complex 1 to the center of complex 2. The brackets $\langle\cdots\rangle$ denote thermal averaging. The mean force is defined in such a way that one has $F_{\text{int}}<0$ in the case of attraction.

The upper half of Fig. 4 shows exemplarily one of the ten sets of the force distance relation between complexes for the case $\kappa=0.4\sigma^{-1}$; the other values are given by Table I. The mean forces determined by the simulation are represented by the small symbols. The curve plotted through the data points shows the least squares fit obtained by fitting the data by the product of an exponential and a rational function.

The resulting ten functions were averaged and the resulting function was integrated to obtain the pair potential function $V(r)$ for a given salt concentration. From the ten functions the statistical error for the parameters was estimated and used to calculate the thinner lines above and below the potential of mean force that indicate the statistical error of the potential itself, cf. Fig. 4.

From the pair potential we calculated A_2 via

$$A_2 = 4v_0 + 2\pi\int_{2a}^{\infty}[1-\exp(-V(r)/kT\,]r^2dr \tag{12}$$

with v_0 denoting the excluded volume of the core sphere. For each salt concentration we obtained ten independent values of A_2 that allowed us to estimate the statistical error.

As can be seen from the example provided in Fig. 4 there is a range of distances where the mean force between the colloids is negative, i.e., where the colloids attract. As a consequence the potential features a minimum. In Fig. 4 we also provide a comparison to the system of two tailless spheres that carry the same net charge as the eight-tail colloids, namely $-Z+8\times10=-70$. Within the DH approximation this case does of course not show any attraction as can be seen by

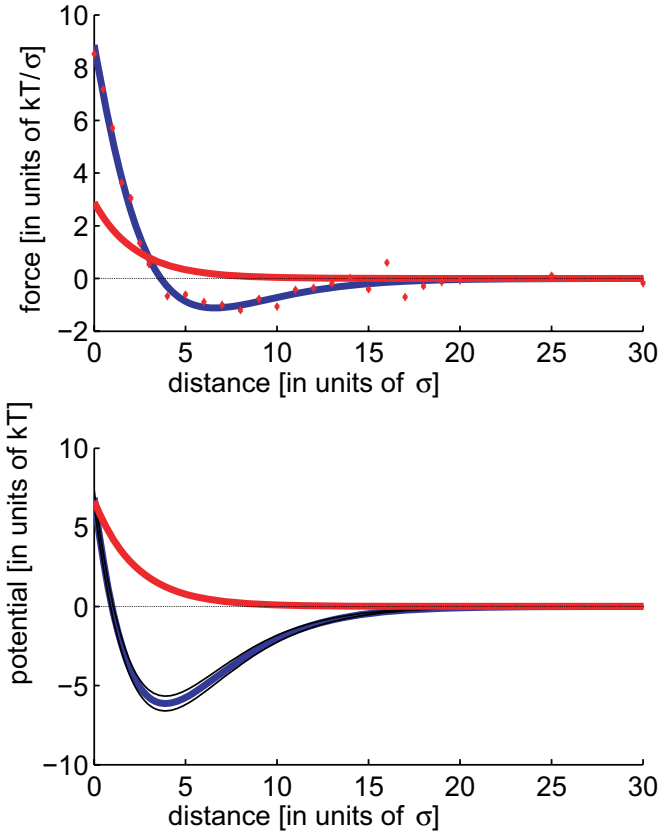

FIG. 4. (Color online) Mean force and resulting pair potential between two complexes. Top: force as a function of surface-surface separation of the cores for $\kappa\sigma=0.4$. The symbols represent the measured mean force, the line shows a mean square fit. Bottom: pair potential between two complexes obtained via integration and averaging over a sample of fitted force functions. For comparison also depicted are the force-distance and potential-distance curves (red) for two charged spheres without tails that carry the net charge $Z=70$ of the eight-tail colloid.

inspecting Eq. (7) with $Z=70$ which is depicted as the red curve at the bottom of Fig. 4. In the following we will investigate closely the mechanism that leads to the attraction between eight-tail colloids.

A. Eight-tail colloid

The inlay of Fig. 5 presents the pair potentials between two complexes, obtained via the procedure described above. The different curves correspond to four different values of κ as explained in the caption of the figure. For all four values we find an attractive potential with a minimum of a few k_BT. Remarkably the depth of the potential shows a nonmonotonic behavior with κ with the maximal value around $\kappa\sigma=0.3$.

From the potentials determined for different values of κ we obtain A_2 as a function of κ that is also depicted in Fig. 5. Not surprisingly, the nonmonotonic dependence of the potential depth with κ is reflected by a nonmonotonic dependence of A_2 with a minimum around $\kappa\sigma=0.3$.

Apparently, the attraction is based on electrostatics. But what is the physical mechanism underlying this attraction? In

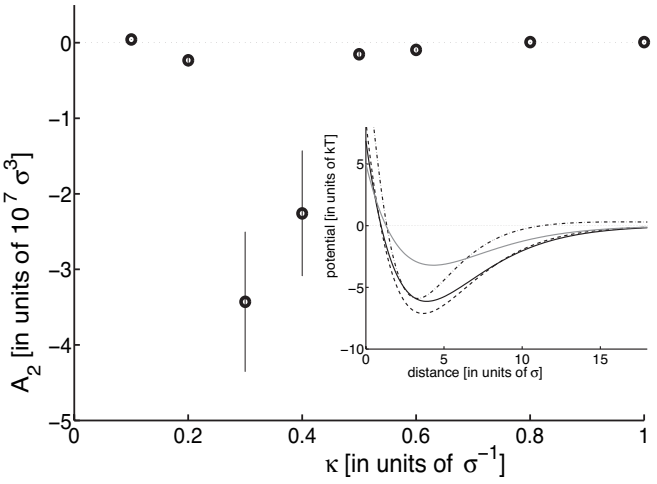

FIG. 5. A_2 of the multi chain complex. The inlay shows the pair potential of two multichain complexes as a function of the surface distance for different values of κ. The values for κ are $0.2\sigma^{-1}$ (black solid), $0.3\sigma^{-1}$ (black dashed), $0.4\sigma^{-1}$ (black dot-dashed), and $0.6\sigma^{-1}$ (gray solid).

principle, there are two mechanisms that could cause the attraction: Patchiness or tail bridging. Our eight-tail colloid might be interpreted—in a coarse-grained spirit—as a colloid with eight charge patches and the correlation between those patches might cause the attraction. Or, if only one tail is actually causing the attractive effect, the number of tails is to a large extent irrelevant and attraction might be based on the bridging of the corresponding tail.

To find out the characteristics of these two mechanisms we introduce here two colloid models that are simpler than the eight-tail colloid and that should show the two different effects in a clean fashion: a colloid with patches but no tails is one model, the other is a colloid that features just a single tail. In the next subsection we will demonstrate that both models lead to a nonmonotonic dependence of A_2 on κ as well.

B. Simplified models

We consider first a colloid with patches. This colloid is obtained by removing the eight tails and just leaving the eight grafted monomers. Each of those monomers carries now the total charge of its former tail, i.e., a charge +10. That means that the eight-patch colloid has the same total charge as the eight-tail colloid.

The pair interaction potential of two such eight-patch colloids is presented in the inset of Fig. 6. The different curves represent different values of κ, as indicated in the caption text. For all investigated values of κ we find a minimum in the potential that for the case $\kappa\sigma=0.2$ is only a local minimum. The minima are now at smaller surface-surface separations of the colloids as compared to the eight-tail complexes. Remarkably, also the eight-tail complex shows a nonmonotonic dependence of the depth of the potential minimum on κ and as a result a nonmonotonic behavior of A_2, cf. Fig. 6. The minimum of A_2 is again around "physiological" conditions $\kappa a=6$ ($\kappa\sigma=0.4$). This might suggest that the at-

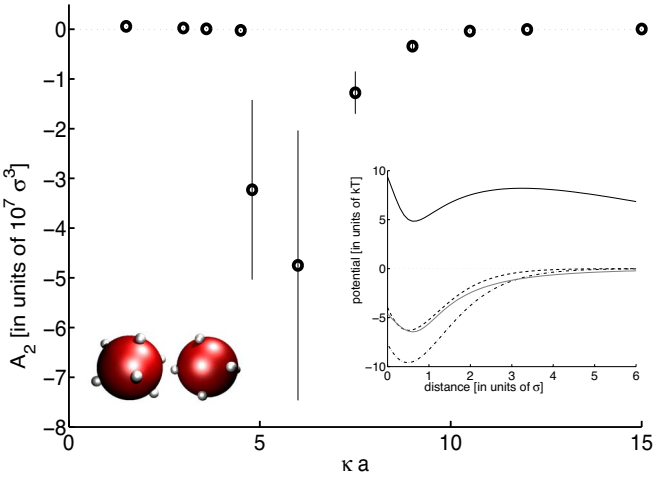

FIG. 6. (Color online) A_2 of the patch model. The inlay shows the pair potential of two patch complexes as a function of the surface distance for different values of κ. The values for κ are $0.2\sigma^{-1}$ (black solid), $0.3\sigma^{-1}$ (black dashed), $0.4\sigma^{-1}$ (black dot-dashed), and $0.6\sigma^{-1}$ (gray solid).

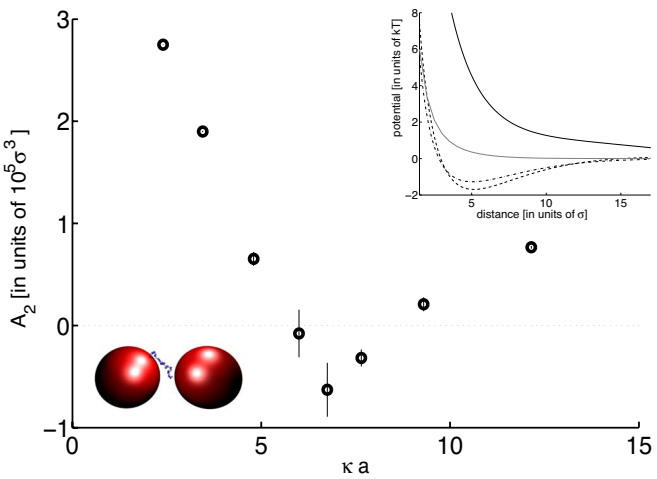

FIG. 7. (Color online) A_2 of the single chain model. The inlay shows the pair potential of two single chain complexes as a function of the surface distance for different values of κ. The values for κ are $0.23\sigma^{-1}$ (black solid), $0.40\sigma^{-1}$ (black dashed), $0.51\sigma^{-1}$ (black dot-dashed), and $0.81\sigma^{-1}$ (gray solid).

traction between eight-tail colloids is essentially based on correlations between patches with the patches being represented by the tails.

To see whether a similar effect can also occur in the absence of patches we consider next the interaction between a one-tail colloid and a colloid without a tail. This way we make sure that no correlation effects between different tails can occur. More specifically, the single-tail colloid is derived from the eight-tail colloid by removing seven tails and adding the charges of those seven tails to that of the central sphere that now carries a charge $-Z+7\times 10$. The charge of the tailless sphere is $-Z+8\times 10$, i.e., both colloids carry the same charge as the eight-tail colloids. We enforce—to achieve better statistics—that the grafting point of the tail is always pointing towards the other colloid and determine the interaction between the single-tail colloid and the tailless colloid.

The inset of Fig. 7 shows the pair potential for this system that features for intermediate salinity, $\kappa\sigma=0.4$ and $\kappa\sigma=0.5$ a minimum whereas for smaller and larger values of κ the potential is purely repulsive. Consequently A_2 as a function of κ also has a nonmonotonic behavior with a minimum around $\kappa\sigma\approx 0.5$. In this model we eliminated any influence of patchiness due to multiple tails, so the attraction that we observe here is mediated by the single tail present in the system.

To conclude, both mechanisms, correlation between patches and tail bridging induce attraction with a nonmonotonic dependence on the salt concentration. What is then the mechanism underlying the attraction between eight-tail colloids?

C. Range of the interaction

In this subsection we provide a criterion that allows to distinguish between correlation of patches and tail bridging: the decay of the potential at larger distances.

The upper row of graphs in Fig. 8 display semilogarithmic plots of the attractive part of the pair potential between eight-tail colloids for different values of κ. The straight lines represent a simple exponential function $C\cdot\exp(-\kappa r)$ which decays with the DH screening length. Here C is chosen such that the line passes through the minimum of the potential. For $\kappa a=3.0$ the potential decays faster than the electrostatic screening but for larger values, especially for $\kappa a=6.0$ and $\kappa a=9.0$ it decays slower than the normal electrostatic screening. This effect is a strong indication that it is in fact tail

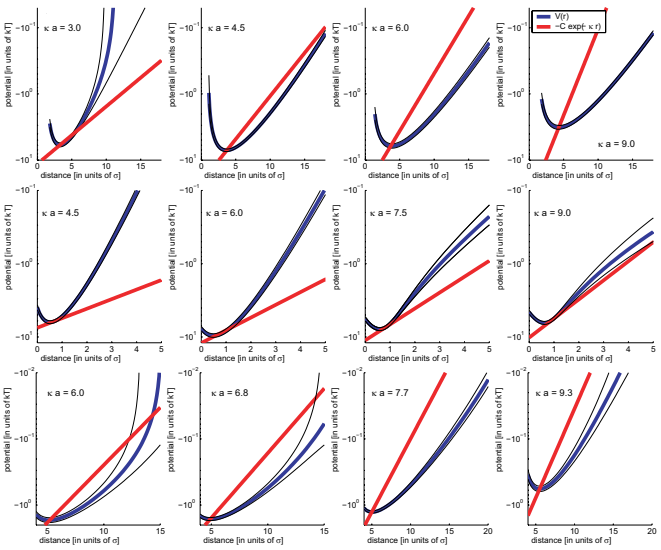

FIG. 8. (Color online) Range of the interaction. The upper line of plots represent the attractive part of the pair interaction of the full chain model on a logarithmic scale for different values of κ as indicated by the labels. The red line indicates the impact of the screening and is proportional to $-C\exp(-\kappa d)$. The plots in the middle and at the bottom represent the patch model and the single chain model, respectively.

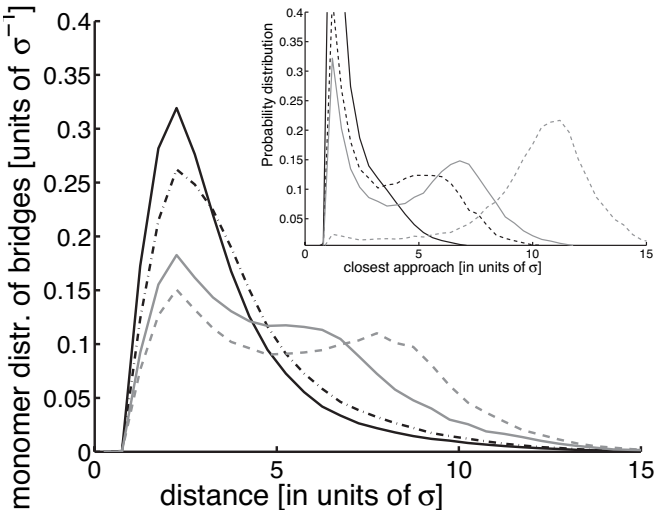

FIG. 9. Monomer density of bridges for different values of the surface-surface separation. The values are $d=0$ (solid black line), $d=4\sigma$ (black dot dashed line), $d=7\sigma$ (gray solid line), and $d=9\sigma$ (gray dashed line). For $d=9\sigma$ the distribution shows two maxima, indicating the preference of the monomers to stay on the surface of one of the charged cores. The inlay shows the probability distribution of the closest approach of a monomers to the alien core for $d=6\sigma$ (solid line), $d=8\sigma$ (black dashed line), $d=9\sigma$ (grey solid line), and $d=13\sigma$ (gray dashed line); see text for details.

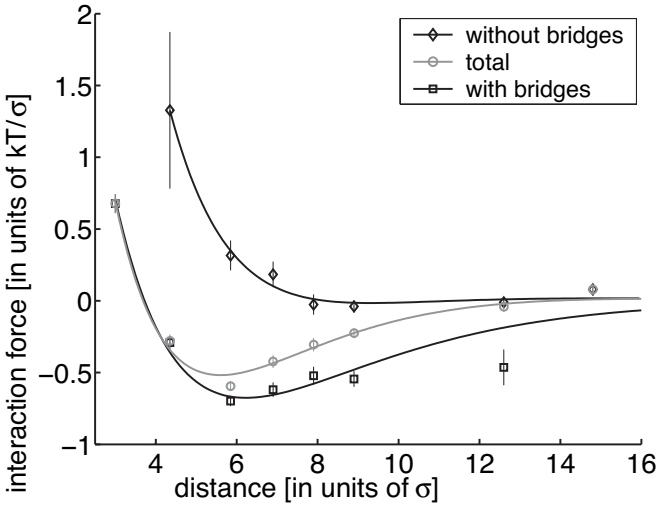

FIG. 10. Separation of the total average of the interaction force (circle) into the part stemming from configurations that feature bridges (squares) and nonbridging configurations (diamonds).

bridging that underlies the attractive interactions observed in the eight-tail colloids.

To check this we show in the middle row of plots in Fig. 8 the attractive part of the pair potential between eight-patch colloids. Clearly, in all cases the potential decays much faster than electrostatic screening $C\cdot\exp(-\kappa r)$ that is also provided in each plot. Apparently patchiness leads to an attraction with a decay length smaller than κ^{-1}. Finally, the last line of plots represent the single chain model for κ values where one has attraction. Also here is a clear indication of a slower decay of the potential as for pure electrostatics.

To conclude, the evidence based on the range of the attractive interaction points clearly towards tail bridging as the dominant mechanism that leads to attraction between eight-tail colloids. In the next section we will focus on details of the bridge-forming tails.

V. TAIL BRIDGING

In this section we take a closer look at the tail bridging mediated attraction. Figure 9 displays monomer distributions for different surface-surface separations of the two colloids. The inset of Fig. 9 presents the density distribution of a special monomer, namely the one of all the 16 tails that—for a given configuration—is closest to the surface of the other colloid. The X axis represents the distance of this monomer to the surface of the other colloid. A nonvanishing value of that monomer density at a small distance signals the occurrence of bridges. The curve in the inlay that corresponds to a surface-surface separation of 13σ does show a broad peak around 11σ reflecting the fact that most of the time all the monomers stay close to their home core and that there is no bridging. With decreasing separation between the colloids a second peak at very small distances appears that reflects the occurrence of bridges where the monomer of closest approach is found nearby the surface of the other colloid. This peak grows at the expense of the other peak when the colloids get closer which demonstrates the increasing occurrence of bridging. Note that for intermediate surface-surface separations there is a minimum in the density distribution around 3.6σ. This allows us to establish a criterion to identify tails that form a bridge: we define a bridge-forming tail as a tail where at least one of its monomers has a separation from the alien colloidal surface that is smaller than 3.6σ.

The main plot of Fig. 9 presents the distribution of all the monomers of such bridge-forming tails for different values of the surface-surface separation of the cores. For small distances between the cores there are almost always bridges. The monomer distribution of the tails shows a strong peak around a distance of 2.5σ. This peak can also be seen at much larger distances like $d=7\sigma$ and $d=9\sigma$. For such large distances the distribution is, however, bimodal. The peak at short distances (around 2.5σ) reflects condensation of tail monomers on the home core whereas the second peak at larger distances can be attributed to condensation on the other core. The bimodal monomer distributions of bridges contrast that of "normal" tails that is shown in Fig. 3.

Figure 10 shows the pair interaction force between two eight-tail complexes (circles) and the contribution from tail bridging configurations (squares) and configurations without bridges (diamonds). As can be clearly seen, the tail-bridging configurations are the ones that cause the overall attractive interaction whereas the average interaction of nonbridging configurations is purely repulsive.

We consider next the bond frequency defined as the fraction of time when two colloids show bridged configurations. In Fig. 11 we display for different values of κ—as indicated in the legend—the bond frequency as a function of the surface-surface separation. As can be seen from this plot the

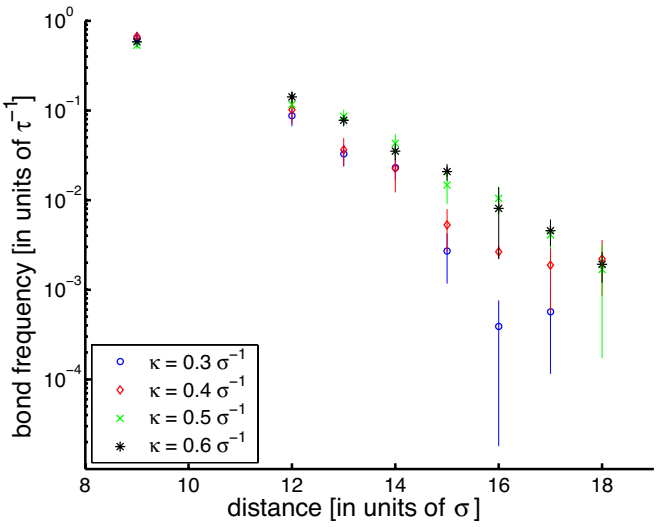

FIG. 11. (Color online) Frequency of bridges as a function of the surface-surface separation for different values of κ.

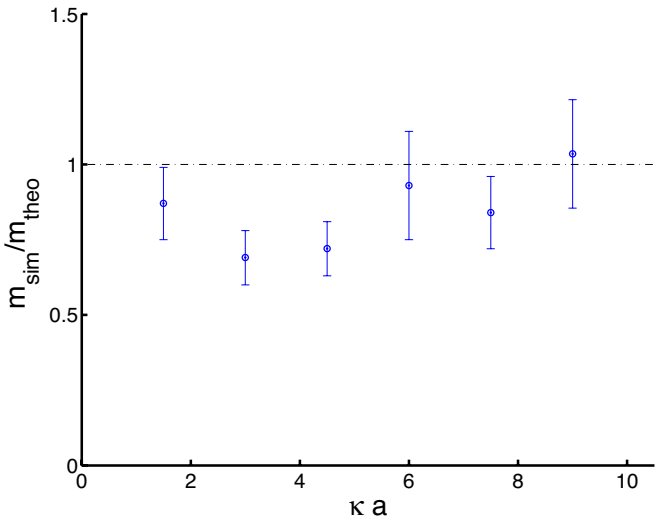

FIG. 12. (Color online) Comparison of the decay parameters m_{sim} obtained from simulated data to our theoretical estimate m_{theo}. See text for details.

frequency shows approximately an exponential decay with distance for $\kappa > 0.3\sigma^{-1}$ and $d > 9\sigma$.

This exponential decay of the bond frequency can be rationalized by a simple physical argument [30]. Monomers that are adsorbed on the home core or the alien core feel an adsorption energy [cf. Eq. (6)],

$$\frac{\epsilon_{ads}}{k_B T} = \frac{V_{DH}^{mc}(\sigma/2)}{k_B T} \approx \frac{V_{DH}^{mc}(0)}{k_B T} = l_B \frac{Z}{a(1+\kappa a)}, \tag{13}$$

where we neglected on the right-hand side the monomer radius.

Two eight-tail colloids that are closer to each other than the contour length of a tail can feature a bridge. The cost of a bridge can be estimated from the number of charged bridge monomers that need to be in between the two cores. These are on the order of $\approx \lambda(d-\kappa^{-1})$ monomers with $\lambda = f/\sigma$ being the line density of the bridge forming tail that is assumed to be stretched out (f: fraction of charged monomers). We thus expect that the probability of finding a bridge, p_{bridge} scales as follows:

$$p_{Bridge} \propto \exp(-\epsilon_{ads}\lambda d/k_B T). \tag{14}$$

We checked Eq. (14) by fitting the bond frequency found in our simulation with an exponential function $g(d) = A \exp(-m_{sim} d)$ with the two parameters A and m_{sim}. Figure 12 shows the ratio of the fitted exponent m_{sim} from the simulated data divided by its predicted value $m_{theo} = \epsilon_{ads}\lambda/k_B T$ as a function of κ. This ratio is indeed always close to 1.

VI. VARIATION OF THE TAIL CHARGE

Equation (14) suggests a strong dependence of the bond frequency on the charge fraction f of the tails. In this section we study in more detail how the pair interaction between eight-tail colloids is affected by a change in the tail charge.

Up to now our tails were 28 monomers long with each third monomer being charged (including the terminal monomers). As a result each tail carried ten charged monomers leading to a charge fraction $f = 10/28 \approx 0.36$. In this section we will use tails with charge fractions ranging from 0.17 to 1. As detailed in Table II we achieve this by changing the numbers of neutral monomers between charged ones. As before we request in addition that the terminal monomers are charged which requires to choose a tail length of either 28 or 29 monomers. In our simulation we always choose $\kappa = 0.4\sigma^{-1}$.

In Fig. 13 we present the pair interaction between two such eight-tail complexes as a function of distance for different values of f. These curves were obtained along the same lines as described in Sec. IV. The overall picture is the following (cf. Fig. 13): With increasing f the minimum of the pair potential becomes deeper and moves to smaller distances. Remarkable is especially how sensitive the depth of the pair potential depends on f: The potential depth for our canonical value $f = 0.36$ is around $-5k_B T$ and that for $f = 0.28$ is around $-1k_B T$, i.e., the reduction by two monomers per tail nearly erases the minimum. In fact, for $f = 0.17$ the minimum has totally disappeared. As we will suggest in the concluding section, it is that strong sensitivity of the interac-

TABLE II. The charge fraction of the tails is varied by changing the number of charged monomers. The table presents the charge fraction, the number of charged monomers, the total number of monomers, and the number of neutral monomers between two consecutive charged monomers for the investigated cases.

Charge fraction	Charged monomers	Total monomers	Neutral monomers between charges
0.17	5	29	6
0.28	8	29	3
0.36	10	28	2
0.52	14	29	1
1.00	28	28	0

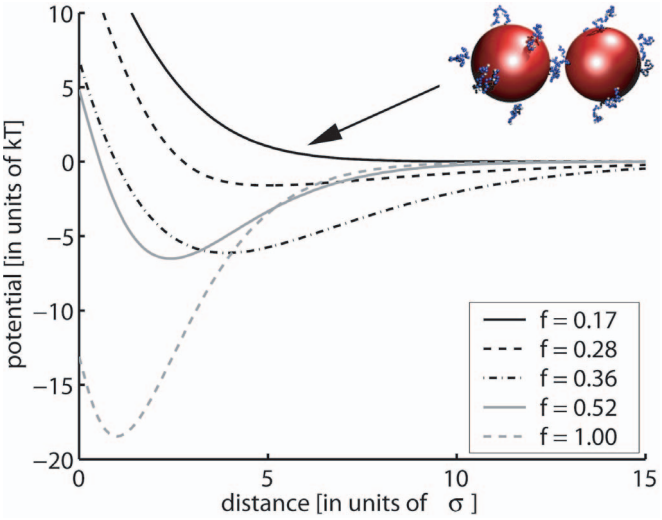

FIG. 13. (Color online) Interaction potential as a function of the surface-surface separation for $\kappa\sigma=0.4$ and different charge fractions f of the tails. Also shown is a typical configuration for weakly charged tails, $f=0.17$.

tion on single tail charges that is used by the cellular machinery as one mechanism to control the compaction of DNA inside chromatin.

In Fig. 14 we plot the equilibrium distance for two eight-tail colloids as a function of the charge fraction f for those f values where the pair potential features a minimum, i.e., excluding the case $f=0.17$. For each value of f we depict also a typical configuration of two colloids at the equilibrium distance. As can be seen from those examples there is a gradual change in the configurations from those that feature tail bridging (for smaller f values) to structures where the underlying mechanism for attraction must be of different origin, especially for the case $f=1$. In that case the equilibrium distance is found around 1σ which allows just one monomer

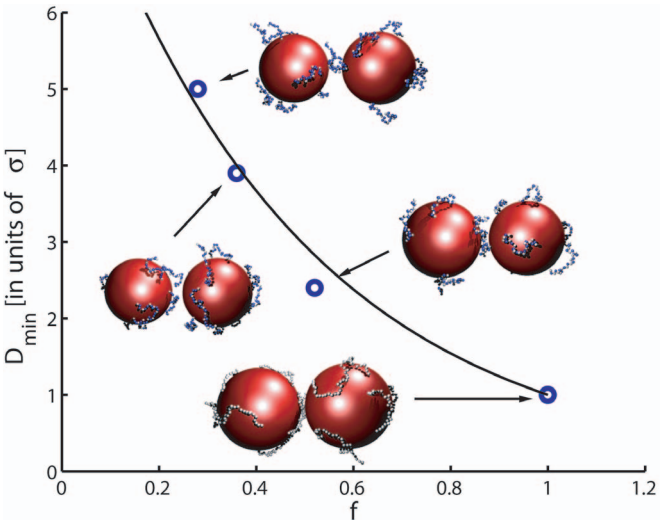

FIG. 14. (Color online) Equilibrium surface-surface separation of two eight-tail colloids as a function of the charge fraction f of the tails. Also shown are example configurations at those optimal distances.

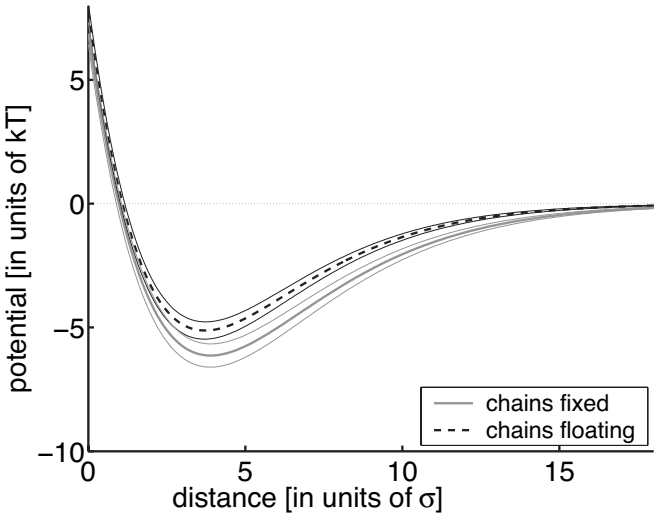

FIG. 15. Pair interaction potential of the floating chain model (dashed line) and that of the eight-tail colloid with fixed grafting points (gray line). Both models feature a minimum of about -5σ at approximately 4σ surface-surface separation. The minimum of the eight-tail colloid is slightly deeper.

to squeeze in between the two colloids. All the tails are tightly adsorbed on the surface of their own cores and are arranged such to mutually avoid each other, hence are strongly correlated. One tail of one colloid is located in the contact area between the two balls. This overall picture is very similar to the patch model discussed in Sec. IV B and the resulting potential with the deep minimum at short distances compares well to the one shown by the patch model, cf. the inset in Fig. 6 that features correlation based attraction.

VII. FLOATING CHAIN MODEL

Up to now we fixed the grafted monomers on the surface and kept also their relative positions fixed, cf. Fig. 1. One might ask how the interaction between the colloids changes when one changes the relative positioning of the grafting points. In this section we will pursue a slightly different direction and allow the anchored monomer to float freely on the surface of the colloid. Such a situation might be experimentally realized by anchoring charged chains onto an oppositely charged vesicle. Note that this model is similar to a model introduced by Granfeldt *et al.* [24] to investigate the interaction between charged colloids carrying adsorbed polyelectrolytes. In that study the interaction potentials were determined via a Monte Carlo simulation and featured typically an attractive minima that was attributed to chain bridging.

The potential of mean force between two colloids each having eight floating chains is depicted in Fig. 15 and is compared to the one of the eight-tail colloid with fixed tails. For both systems we choose the "canonical" values for all parameters, i.e., $\kappa=0.4\sigma^{-1}$, $f=0.36$, and so on. For the freely floating tails we performed five runs of 2×10^6 time steps with different initial conditions for each data point, allowing us to average the potential over five curves. Remarkably the

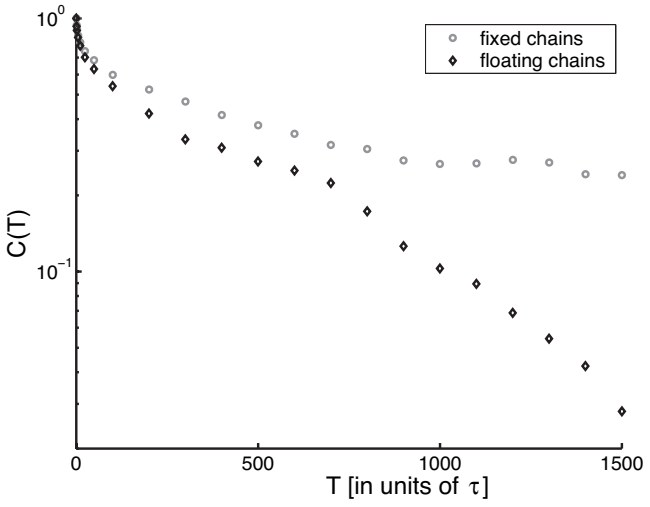

FIG. 16. Correlation function of bridge-forming tails for the two type of models as a function of the LJ time τ for the core-core distance 9σ at $\kappa=0.4\sigma^{-1}$. The correlation times for the fixed chain system is considerably larger than for floating chains.

interaction potentials of the two systems are nearly identical with the fixed tail colloids showing a slightly deeper potential minimum.

This result is surprising since one might have expected that the freely floating chains could take an advantage of their mobility and move into the interaction zone between the colloids. However, due to the mutual repulsion between the tails there is usually not more space than for one bridge. The slightly smaller attraction between the eight-tail colloids might reflect the entropic penalty for the bridge-forming tail that loses its translational degree of freedom.

Differences between fixed and floating tail anchors become more prominent when looking at the correlation times for a bridge-forming tail to stay in the bridge:

$$C(T) = \frac{1}{16}\sum_i \langle P_B^i(t) \cdot P_B^i(t+T)\rangle / \langle P_B^2\rangle \qquad (15)$$

Here $P_B^i(t)$ denotes the probability to find the ith tail of the two complexes forming a bridge at the time t and P_B is the overall probability to find a given tail in a bridge. Figure 16 presents $C(T)$ for the floating and the fixed chain model. The correlation of the floating chain model decays much faster than that of the fixed chain model. This reflects the fact that in the floating chain model a single bridging chain can move out of the bridging region independently from the other chains whereas for the fixed tails this requires a rotation of the whole colloid. Therefore in the latter case a bridging tail stays on average longer in the interaction zone.

VIII. DISCUSSION AND CONCLUSION

We have presented a simplified model of the nucleosome core particle, the eight-tail colloid. We were able to show that—within this model—the interaction between eight-tail colloids is mainly governed by the tails. In accord with the experiments on NCPs performed in Refs. [13–15] we find that the underlying mechanism is tail bridging where typically one tail of one colloid bridges to the other colloid. Other mechanisms like charge correlations show similar behavior like a nonmonotonic dependence of the second virial coefficient on the salt concentration. What is, however, characteristic of tail bridging is an interaction range that can be much longer than that of the screened electrostatics. Of special interest is the strong dependence of the interaction on the fraction of charged tail monomers. Changes by one or two charges on a tail have already a strong impact on the interaction such that the attraction can be switched on and off.

The experiments on histone tail bridging [13–15] as well as our study focus on the interaction between NCPs. In the cell, however, nucleosomes are connected to each other via linker DNA which results in a chromatin fiber. This leads to the question whether tail bridging is also important for nucleosomes in such a fiber.

That this is indeed the case follows from a recent computer simulation [31] where the NCP crystal structure has been mimicked by a cylinder with 277 charge patches (accounting for charged groups on the surface of the NCP) with all the tails anchored to it. By switching on and off the charges on the tails it was found that the tails play a crucial role in the electrostatic nucleosome-nucleosome and nucleosome-linker DNA interaction within that chromatin fiber model—causing the stabilization of the fiber at physiological salt conditions.

As a cautionary side remark we would like to note that it is very much possible that inside chromatin fibers some of the tails play different roles. It was, for instance, suggested that the two H3 tails might be involved in the interaction with the linker DNA thereby controlling the DNA entry-exit angle at the nucleosome [32,33].

As mentioned above, tail bridging is very sensitive to the number of charges on the tails which immediately suggest a possible mechanism to control the interaction between nucleosomes. It is in fact known that the cellular machinery is capable of controlling the charge state of the histone tails via the acetylation (the "discharging") and deacetylation (the "charging") of its lysine groups [3]. Active, acetylated regions in chromatin are more open, inactive, deacetylated regions tend to condense locally and on larger scales as well [34]. The role of acetylation for the genetic expression has been recently demonstrated via *in vivo* experiments [35] on yeast strains that contained mutated H4 tails where the lysines where replaced by arginines that cannot be neutralized. The gene expression of these mutants had been screened for all possible combinations and it was observed that most lysines acted as "charge counters," i.e., the more mutations had been introduced the stronger were the changes in gene expressions. Only one of the four lysine residues in the H4 tail showed a very specific response, presumably recruiting special modification-specific proteins that in turn, e.g., silence a whole region of chromatin. On the other hand, mutations on the other three residues showed an unspecific, cumulative effect. Of interest to our study are especially

clustered chromosomal regions where genetic activity is down-regulated with increasing charge numbers on the tails. This might reflect condensation of the chromatin fibers due to enhanced nucleosomal attraction via tail bridging in that regions.

ACKNOWLEDGMENTS

The authors thank M. Deserno, B. Dünweg, K. Kremer, F. Livolant, S. Mangenot, and R. Podgornik for helpful discussions. Funding from the SFB 625 is gratefully acknowledged.

[1] H. Schiessel, J. Phys.: Condens. Matter **15**, R699 (2003).
[2] K. Luger, A. W. Mader, R. K. Richmond, D. F. Sargent, and T. J. Richmond, Nature (London) **389**, 251 (1997).
[3] P. J. Horn and C. L. Peterson, Science **297**, 1824 (2002).
[4] K. J. Polach and J. Widom, J. Mol. Biol. **254**, 130 (1995).
[5] I. M. Kulic and H. Schiessel, Phys. Rev. Lett. **92**, 228101 (2004).
[6] G. Li, M. Levitus, C. Bustamante, and J. Widom, Nat. Struct. Mol. Biol. **12**, 46 (2005).
[7] M. Tomschik, H. Zheng, K. van Holde, J. Zlatanova, and S. H. Leuba, Proc. Natl. Acad. Sci. U.S.A. **102**, 3278 (2005).
[8] J. M. Gottesfeld, J. M. Belitsky, C. Melander, P. B. Dervan, and K. Luger, J. Mol. Biol. **321**, 249 (2002).
[9] I. M. Kulic and H. Schiessel, Phys. Rev. Lett. **91**, 148103 (2003).
[10] F. Mohammad-Rafiee, I. M. Kulic, and H. Schiessel, J. Mol. Biol. **344**, 47 (2004).
[11] P. B. Becker, EMBO J. **21**, 4749 (2002).
[12] F. Mühlbacher, C. Holm, and H. Schiessel, Europhys. Lett. **73**, 135 (2006).
[13] S. Mangenot, A. Leforestier, P. Vachette, D. Durand, and F. Livolant, Biophys. J. **82**, 345 (2002).
[14] S. Mangenot, E. Raspaud, C. Tribet, L. Belloni, and F. Livolant, Eur. Phys. J. E **7**, 221 (2002).
[15] A. Bertin, A. Leforestier, D. Durand, and F. Livolant, Biochemistry **43**, 4773 (2004).
[16] K. Luger and T. J. Richmond, Curr. Opin. Genet. Dev. **8**, 140 (1998).
[17] H. Boroudjerdi and R. R. Netz, Europhys. Lett. **64**, 413 (2003).
[18] H. Boroudjerdi and R. R. Netz, J. Phys.: Condens. Matter **17**, S1137 (2005).
[19] I. Rouzina and V. A. Bloomfield, J. Phys. Chem. **100**, 9977 (1996).
[20] E. Allahyarov, H. Löwen, J. P. Hansen, and A. A. Louis, Phys. Rev. E **67**, 051404 (2003).
[21] R. Podgornik, J. Chem. Phys. **118**, 11286 (2003).
[22] T. Åkesson, C. Woodward, and B. Jönsson, J. Chem. Phys. **91**, 2461 (1989).
[23] S. J. Miklavic, C. E. Woodward, B. Jönsson, and T. Åkesson, Macromolecules **23**, 4149 (1990).
[24] M. K. Granfeldt, B. Jönsson, and C. E. Woodward, J. Phys. Chem. **95**, 4819 (1991).
[25] R. Podgornik, T. Åkesson, and B. Jönsson, J. Chem. Phys. **102**, 9423 (1995).
[26] K. Kremer and G. S. Grest, J. Chem. Phys. **92**, 5057 (1990).
[27] D. A. McQuarrie, *Statistical Mechanics* (Harper-Collins, New York, 1976).
[28] S. Alexander, P. M. Chaikin, P. Grant, G. J. Morales, P. Pincus, and D. Hone, J. Chem. Phys. **80**, 5776 (1984).
[29] D. Frenkel and B. Smit, *Understanding Molecular Simulation*, 2nd edition (Academic Press, San Diego, 2002).
[30] H. Schiessel, Eur. Phys. J. E **19**, 251 (2006).
[31] J. Sun, Q. Zhang, and T. Schlick, Proc. Natl. Acad. Sci. U.S.A. **102**, 8180 (2005).
[32] J. Zlatanova, S. H. Leuba, and K. van Holde, Biophys. J. **74**, 2554 (1998).
[33] H. Schiessel, Europhys. Lett. **58**, 140 (2002).
[34] C. Tse, T. Sera, A. P. Wolffe, and J. C. Hansen, Mol. Cell. Biol. **18**, 4629 (1998).
[35] M. F. Dion, S. J. Altschuler, L. F. Wu, and O. J. Rando, Proc. Natl. Acad. Sci. U.S.A. **102**, 5501 (2005).